

UC Santa Cruz

UC Santa Cruz Electronic Theses and Dissertations

Title

Synthesis, Structure, and Fluorescence Behavior of Profluorescent 8-amino BODIPY Nitroxides

Permalink

<https://escholarship.org/uc/item/2xb2v7dv>

Author

Schultz-Simonton, Wiley

Publication Date

2019

Peer reviewed|Thesis/dissertation

UNIVERSITY OF CALIFORNIA

SANTA CRUZ

Synthesis, Structure, and Fluorescence Behavior

of Profluorescent 8-amino BODIPY Nitroxides

A thesis submitted in partial satisfaction of the requirements for the degree of

MASTER OF SCIENCE

in

CHEMISTRY

by

Wiley Schultz-Simonton

March 2019

The Thesis of Wiley
Schultz-Simonton is approved:

Professor Rebecca Braslau, Chair

Professor Scott Oliver

Professor Bakthan Singaram

Lori Kletzer

Vice Provost and Dean of Graduate Studies

TABLE OF CONTENTS

Abstract	1
Acknowledgements	2
Introduction	3
Results and Discussion	4-6
Conclusion	6-7
Experimental Section	7-11
Tables and Figures	12-14
Figure 1	12
Figure 2	12
Scheme 1	12
Figure 3	13
Table 1	14
References	15-16
Appendix	17-39
I. Absorption and emission spectra for compounds 1-6	17-18
II. General Methods	19
III. Crystallographic details 1, 2, and 3	20-28
IV. ¹H NMR spectra for 1-6	29-34
V. ¹³C NMR spectra for 1-6	35-40
VI. References	41

ABSTRACT

Synthesis, Structure, and Fluorescence Behavior
of Profluorescent 8-Amino BODIPY Nitroxides

Wiley Schultz-Simonton

A series of novel 8-amino BODIPY profluorescent nitroxides and the corresponding *N*-ethoxyamine derivatives were synthesized with varying substitution and molecular geometries. Single crystal X-ray diffraction data for the three 8-amino BODIPY nitroxides were obtained. UV-Vis absorption and emission data for the profluorescent nitroxides and 8-amino BODIPY *N*-ethoxyamine derivatives were examined to assess the utility of these compounds as fluorescent probes.

ACKNOWLEDGEMENTS

Acknowledgement to the Gura family for funding which made this research possible.

Special thanks to my advisor Rebecca Braslau, for mentorship, advocacy, and support through a difficult but incredibly enriching experience.

The text of this thesis includes reprint of the following previously published material: [Synthesis, Structure, and Fluorescence Behavior of Profluorescent 8-Amino BODIPY Nitroxides, Wiley Schultz-Simonton, Patrick Skelly, Indranil Chakraborty, Pradip Mascharak, Rebecca Braslau*, *European Journal of Organic Chemistry*, Volume **2019**, Issue 7, pp]. I thank Dr. Indranil Chakraborty and Professor Pradip Mascharak for obtaining the X-ray data.

INTRODUCTION

“Profluorescent nitroxides” are fluorescent dyes covalently bonded to a persistent nitroxide radical. Interaction between the radical and the excited state of the fluorophore results in a suppression of the fluorescence emission, occurring both in cases where the nitroxide is covalently bound (intramolecular) and where separate nitroxide and fluorophore molecules have sufficient proximity to form an “encounter complex” (intermolecular). This property, along with the reversible redox properties and unique reactivity of the nitroxide group, allows for design of fluorescent probes which have been utilized to visually monitor a variety of processes which involve redox changes and/or radical intermediates.¹

The quenching effect observed with profluorescent nitroxides is attributed to an electron exchange process; the unpaired electron provides a “spin-allowed” nonradiative decay mechanism for the fluorophore excited-state.² The strength of this fluorescence quenching is influenced by proximity of the fluorophore to the nitroxide radical,³ and is enhanced in cases where the nitroxide and fluorophore are π conjugated and/or attached by rigid C–C bonds rather than flexible linkages.⁴ However, synthetic routes to such compounds can be cumbersome,⁵ thus synthesis involving accessible 2,2,6,6-tetramethyl-piperidine-1-oxyl (TEMPO) derivatives is appealing for probe design. Relatively little is understood about the precise geometric parameters important in designing profluorescent nitroxides with high quenching efficiencies.¹

To better understand the molecular and environmental properties that lead to efficient fluorescence quenching, the syntheses of profluorescent 8-amino BODIPY nitroxides **1**, **2**, and **3** and their fluorescent *N*-ethoxyamine analogs **4**, **5**, and **6** (**Figure 1**) was undertaken based on methodology developed by Bañuelos.^[7] In general, BODIPY dyes have high photo- and chemical stability, “tunable” excitation and emission wavelengths ($\lambda_{em}/\lambda_{ex}$), large extinction coefficients (ϵ) and high fluorescence quantum yields (ϕ)^{6,8} making them attractive for a wide variety of sensing applications.^{5,8,9} Profluorescent nitroxides **1**, **2**, and **3** were selected for their differences in predicted geometries and $\lambda_{em}/\lambda_{ex}$, to explore the effects of variable bond angles and distances on spectroscopic properties. Their usefulness as probes is essentially a function of the ratio of fluorescence quantum yield ϕ between the *N*-ethoxyamine and the corresponding nitroxide: $\phi_{NOEI}/\phi_{NO\cdot}$.

RESULTS AND DISCUSSION

Profluorescent nitroxides **1**, **2**, and **3** were obtained in modest to moderate yield by treatment of the corresponding 8-methylthio BODIPY with 4-amino TEMPO using methodology developed by Bañuelos et al. (**Scheme 1**).^{7,12} Tetramethyl nitroxide **3** was recovered in the lowest yield, presumably due to a more sterically crowded reactive site in precursor **9**. The nitroxides were converted in modest to poor yields to the corresponding *N*-ethoxyamines in unoptimized reactions by treatment with excess triethylborane and slow introduction of air. Particularly low recoveries were achieved for *N*-ethoxyamine **4**, perhaps due to a competing Minisci type reaction at the unsubstituted α position of the BODIPY pyrrole ring.

BODIPY dyes with an 8-amino substituent can be drawn as one of two resonance structures: the “cyanine” and “hemicyanine” forms (**Figure 2**). For the electron density on the central nitrogen to delocalize significantly into the BODIPY

system, the lone pair must adopt a coplanar orientation to the conjugated system. In sterically crowded compounds such as **3**, the nitrogen is precluded from overlap by geometric constraints, whereas in **1** and **2**, the central nitrogen is less sterically constrained and is able to contribute significant cross-conjugated hemicyanine character.

The molecular structures and selected atomic bond angles and interatomic distances from X-ray data are shown in **Figure 3**. Consistent with earlier studies on 8-amino BODIPY dyes,² sterically unhindered nitroxide **1** has a central nitrogen optimally oriented for π bonding with a small $C^3-N^2-C^{10}-C^{11}$ dihedral angle of 3.1° , and a shortened $C^{10}-N^2$ bond length indicating a rigid hemicyanine structure. Also, consistent with significant hemicyanine character is the presence of six nonequivalent pyrrolic protons in the 1H NMR, and no symmetry in the pyrrolic ^{13}C signals for both **4** and **1**. In contrast, nitroxide **3** adopts a near perpendicular orientation between the BODIPY plane and the TEMPO moiety, and symmetry is observed in both the proton and carbon NMR spectra for the pyrrolic system. Nitroxide **2** adopts a conformation intermediate between **1** and **3** with symmetrical pyrrole signals in the NMR spectra, suggesting unhindered rotation about the $C^{11}-N^2$ bond in CD_3OD as in **3**. Unlike nitroxide **3**, **2** has significant hemicyanine character as evidenced by the central C-N bond lengths similar to those of **1**, and a significant hypsochromic shift in λ_{ex} and λ_{em} relative to unsubstituted compounds **1** and **4**. The distances between the nitroxide nitrogen atoms N^1 and the BODIPY fluorophore is shortest in **3**, where the TEMPO ring adopts an almost perpendicular orientation to the BODIPY π system, compared to slightly longer central C-N bond lengths in **1** and **2**. No clear correlation between these distances from the crystal structures and fluorescence quenching efficiencies was observed, with the dimethyl compound **2** displaying the largest $\phi_{NOEt}/\phi_{NO^\bullet}$.

The $\lambda_{em}/\lambda_{ex}$ and other spectroscopic properties of the nitroxides and corresponding ethoxyamines are summarized in **Table 1**. Each dye shows a hypsochromic shift in λ_{ex} going from nonpolar CyH/ CH_2Cl_2 to polar MeOH solvent.

This effect is most pronounced in dyes **1**, **2**, **4**, and **5** with significant hemicyanine character. The λ_{em} are not significantly affected, which suggests the shift arises from (de)stabilization of the ground state rather than effects on the structures excited states. The Stokes shift decreases in the order **1** \approx **4** > **2** \approx **5** > **3** \approx **6**. The fluorescence efficiency ratios $\phi_{NOEI}/\phi_{NO\cdot}$ between *N*-ethoxyamine and corresponding nitroxide are summarized in **Table 1**, as well as the effective fluorescence efficiency ratios $\phi_{NOEI}/\phi_{NO\cdot}$ (0.1 mM). This value is not a true quantum yield, as the relation between absorption and emission deviates significantly from linearity at this concentration, due to reabsorption and inner filter effects. However, this value is of interest in considering the utility of the dyes in sensing applications which may require high dye loading. The fluorescence efficiencies of the nitroxides are significantly lower than the *N*-ethoxyamine counterparts, as expected. However, nitroxide **1** displayed a slightly higher fluorescence efficiency than its *N*-ethoxyamine derivative **4** in MeOH solvent. Low fluorescence has been observed for similar 8-amino BODIPYs in polar media, previously attributed to intramolecular charge transfer (ICT) quenching.^{2,3,7} However, the solvent dependence on fluorescence quantum yield shown by *N*-ethoxyamine **4** is absent in nitroxide **1**, which shows similar ϕ in MeOH and CyH/CH₂Cl₂. Evidently, in **1**, the quenching effect of the pendant nitroxide outweighs the enhancement in ICT rate afforded by the increase in solvent polarity. *N*-ethoxyamine **5** shows less solvent dependence, and the effect of solvent on ϕ is reversed in nitroxide **2**. The fluorescence of nitroxide **3** and *N*-ethoxyamine **6** appear relatively insensitive to solvent polarity. At higher concentration, differences in the quenching abilities of the dyes are more distinctive; $\phi_{NOEI}/\phi_{NO\cdot}$ is enhanced at high concentration in most cases, but actually decreases for **2** in CyH/CH₂Cl₂. The $\phi_{NOEI}/\phi_{NO\cdot}$ (0.1 mM) = 130 is very large for nitroxide **3** in CyH/CH₂Cl₂, which suggests the tetramethyl probe may be the most useful of these profluorescent nitroxides as a sensor (which may require high dye concentration). Solid state fluorescence was also observed for **3** and **6**, a property which may have utility in development of visualization techniques using

profluorescent nitroxides. The approximately perpendicular orientation of the TEMPO group with respect to the BODIPY fluorophore may disrupt stacking and other intermolecular interactions known to suppress fluorescence, which occur both at high concentration and in the solid.

The on/off fluorescence performance of the dyes examined here is comparable with previously synthesized tetramethyl substituted BODIPY profluorescent nitroxides where C-C linkages are used.^{13a,13b,17} The $\phi_{N\text{-alkoxyamine}}/\phi_{\text{NO}^+}$ for *meso* substituted profluorescent nitroxides **1–3** is also on par with that found for isoindoline BODIPY nitroxides with C-C linkages.⁵ The performance of these new dyes is significantly better than previously synthesized BODIPY TEMPO conjugates using phenyl “spacers,” utilizing alkyne–azide cycloaddition,¹⁴ ester¹⁵ or amide¹⁶ linkages to attach the BODIPY and TEMPO moieties. This methodology for formation of the critical C-N linkages is efficient and allows for shorter distances between the nitroxide radical center and the BODIPY core.

CONCLUSION

Synthesis and spectroscopic analysis of three novel profluorescent BODIPY nitroxides and their *N*-ethoxyamine analogues was carried out, to assess their fluorescence behavior and usefulness as probes. X-ray diffraction for the three nitroxide probes was analyzed and molecular geometry correlated to fluorescence characteristics. BODIPY **1** exhibits a nearly coplanar relation between the TEMPO moiety and the BODIPY system and asymmetry in the NMR signals, indicating a largely cross-conjugated hemicyanine character. Dye **3** has a nearly perpendicular orientation between the TEMPO and BODIPY moieties, and a hypsochromic shift in $\lambda_{\text{em}}/\lambda_{\text{ex}}$ that suggests a dominant cyanine resonance contribution. Dye **2** has symmetry in the NMR signals of the BODIPY rings (indicating free rotation about the central C-N bond), but $\lambda_{\text{em}}/\lambda_{\text{ex}}$ intermediate between **1** and **3**, suggesting this dye has significant hemicyanine resonance contribution as in **1**. The fluorescence of

N-ethoxyamine **4** shows dramatic sensitivity to solvent polarity that is absent in nitroxide precursor **1**. Dyes **5** and **2** show a fairly large $\phi_{\text{NOEI}}/\phi_{\text{NO}^{\bullet}}$, and distinct responses to solvent polarity between nitroxide and *N*-ethoxyamine. No clear trend relating nitroxide-fluorophore distance to $\phi_{\text{NOEI}}/\phi_{\text{NO}^{\bullet}}$ was obvious, although these interesting and unexpected results observed may lead to better design of profluorescent nitroxides in the future. The solid-state fluorescence and good performance at high concentrations of nitroxide **3** should be valuable in visual sensing applications.

EXPERIMENTAL SECTION

All reagents and solvents were used as received unless otherwise noted. Dry CH_2Cl_2 was obtained by refluxing over CaH_2 and storage over 4Å molecular sieves. Toluene, CH_2Cl_2 , CH_3CN , MeOH, and THF were supplied by Fisher. Diethyl ether, $\text{BF}_3\cdot\text{OME}_2$, $\text{BF}_3\cdot\text{OEt}_2$, CaH_2 , cyclohexane and thiophosgene (85%) were supplied by Acros Organics. Ascorbic acid, 1 M BEt_3 in hexanes, and 1 M BEt_3 in THF were supplied by Sigma Aldrich. 4Å Molecular sieves and pyrrole were supplied by Alfa Aesar. Methyl iodide was supplied by Spectrum. 2-Methylpyrrole was supplied by BePharm Limited. 2,4-Dimethylpyrrole was supplied by TCI. TLC analysis was performed on 0.20 mm silica gel 60 plates with UV_{254} , supplied by Macherey-Nagel. Deuterated solvents CD_3OD , C_6D_6 , and CDCl_3 were supplied by Cambridge Isotope Laboratories.

Preparation of 4-amino-2,2,6,6 tetramethylpiperidin-1-oxyl (4-amino TEMPO) was carried out by the method of Zagatto et al.^[10] BODIPYs **7**, **8**, and **9** were synthesized according to the procedure of Biellmann.^[11]

8-*N*-(1-Oxyl-2,2,6,6-tetramethyl-4-piperidinyI)-4,4-difluoro-4-bora-3a,4a-diaza-s-indacene (BODIPY-amino-TEMPO 1): Following a modified literature procedure,^[7] to a dry round-bottomed flask equipped with a stir bar was charged 50 mg (0.21 mmol, 1.0 eq.) of 8-methylthio BODIPY **7**, dissolved in 10 mL of freshly

distilled CH₂Cl₂ and stirred for 10 minutes before adding 60 mg (0.35 mmol, 1.7 eq.) of 4-amino-TEMPO. The mixture was capped and allowed to stir for 22 h, after which TLC analysis showed consumption of **7**. The mixture was evaporated in vacuo and the residue purified by flash chromatography on SiO₂ (gradient: CH₂Cl₂ to CH₂Cl₂/MeOH, 96:4) to give 70 mg (90% yield) of **1** as an orange powder, mp = 256–257° C. *R*_f = 0.21 (99:1 CH₂Cl₂/MeOH). ¹H NMR (500 MHz, CD₃OD, ascorbic acid added in situ) δ = 7.55 (s, 1H), 7.41 (s, 1H), 7.35 (s, 1H), 7.32 (s, 1H), 6.57 (s, 1H), 6.38 (s, 1H), 4.57 (tt, 1H, *J* = 12.0 Hz, 3.5 Hz), 2.11 (m, 2H), 1.90 (t, 2H, *J* = 12.0 Hz), 1.33 (s, 6H), 1.26 (s, 6H). ¹³C NMR, HSQC (125 MHz, CD₃OD, ascorbic acid added in situ) δ = 149.8 (4°), 135.0 (CH), 132.6 (CH), 126.9 (4°), 123.3 (CH), 123.2 (4°), 117.9 (CH), 115.2 (CH), 114.2 (CH), 60.8 (4°), 49.9 (CH), 44.5 (CH₂), 32.3 (CH₃), 20.4 (CH₃). IR (cm⁻¹): 3452 (s), 1712 (br, s), 1458 (s), 1378 (m). HRMS (ESI-Orbitrap) *m/z*: (MH + H)⁺ calcd. for (C₁₈H₂₆BF₂N₄O)⁺; 363.2169, found 363.2143.

8-*N*-(1-Oxyl-2,2,6,6-tetramethyl-4-piperidiny)-4,4-difluoro-3,5-dimethyl-4-bora-3a,4a-diaza-*s*-indacene (diMeBODIPY-amino-TEMPO **2):** Following a modified literature procedure,^[7] to a dry round-bottomed flask equipped with a stir bar was charged 20 mg (0.075 mmol, 1.0 eq.) of 8-methylthio dimethyl BODIPY **8**, dissolved in 20 mL of freshly distilled CH₂Cl₂ and stirred for 10 minutes before adding 22 mg (0.13 mmol, 1.7 eq.) of 4-amino-TEMPO. The mixture was capped and left stirring for 3 h, after which TLC analysis showed consumption of **8**. The mixture was evaporated in vacuo and the residue purified by flash chromatography on SiO₂ (gradient: hexanes to CH₂Cl₂/hexanes/MeOH, 47.5:47.5:5) to give 15 mg (51% yield) of **2** as an orange powder, mp = 239–240° C. *R*_f = 0.37 (99:1 CH₂Cl₂/MeOH). ¹H NMR (500 MHz, CD₃OD, ascorbic acid added in situ) δ = 7.22 (d, *J* = 4.0 Hz, 2H), 6.20 (s, 2H), 4.44 (tt, *J* = 3.8 Hz, 12.5 Hz, 1H), 2.47 (s, 6H), 2.07 (dd, *J* = 12.5 Hz, 3.8 Hz, 2H), 1.83 (t, *J* = 12.5 Hz, 2H), 1.30 (s, 6H), 1.25 (s, 6H). ¹³C NMR (125 MHz, CD₃OD, ascorbic acid added in situ) δ = 147.4 (broad), 126.4, 115.5 (broad), 115.4 (broad), 106.9, 60.3, 44.9, 32.5, 20.4, 14.1. IR (cm⁻¹): 3409 (s), 1710 (br, w), 1482

(s), 1365 (m). HRMS (ESI-Orbitrap) m/z : (MH + H)⁺ calcd. for (C₂₀H₃₀BF₂N₄O)⁺; 391.2472, found 391.2457.

8-N-(1-Oxyl-2,2,6,6-tetramethyl-4-piperidiny)-4,4-difluoro-1,3,5,7-tetramethyl-4-bora-3a,4a-diaza-s-indacene (tetMeBODIPY-amino-TEMPO 3): Following a modified literature procedure,^[12] to a round-bottomed flask equipped with a stir bar was charged 305 mg (1.04 mmol, 1.00 eq.) of 8-methylthio BODIPY 9 dissolved in 4 mL of CH₃CN, and 223 mg (1.30 mmol, 1.25 eq.) of 4-amino-TEMPO was added. The mixture was stirred open to air for 21 h, after which TLC analysis showed consumption of 9. The mixture was evaporated in vacuo and the residue purified by flash chromatography on SiO₂ (gradient: 98:2 hexanes/EtOAc to 40:60 hexanes/EtOAc) to give 158 mg (36% yield) of 3 as orange crystals, mp = 192–193° C. R_f = 0.57 (99:1 CH₂Cl₂/MeOH). ¹H NMR (500 MHz, CD₃OD, ascorbic acid added in situ) δ = 6.09 (s, 2H), 3.91 (tt, J = 4 Hz, 12 Hz, 1H), 2.41 (s, 6H) 2.38 (s, 6H), 1.96 (m, 2H), 1.56 (t, J = 12 Hz, 2H) 1.14 (s, 6H), 1.07 (s, 6H). ¹³C NMR (125 MHz, CD₃OD, ascorbic acid added in situ) δ = 149.2, 134.9, 125.8, 119.6, 106.9, 60.3, 56.0, 47.5, 32.7, 20.5, 15.6, 14.2. IR (cm⁻¹): 3431 (s), 1686 (br, s), 1469 (s), 1364 (m). HRMS (ESI-Orbitrap) m/z : (MH + H)⁺ calcd. for (C₂₂H₃₄BF₂N₄O)⁺; 419.2785, found 419.2760.

8-N-(1-Ethoxy-2,2,6,6-tetramethyl-4-piperidiny)-4,4-difluoro-4-bora-3a,4a-diaza-s-indacene (BODIPY-amino-TEMPOEt 4): To a dry round-bottomed flask equipped with a stir bar was charged 11 mg (0.030 mmol, 1.0 eq.) of BODIPY-aminoTEMPO 1 dissolved in 2 mL of THF. The mixture was stirred for 20 min before 50 μ L (0.05 mmol, 1.7 eq.) of 1 M BEt₃ in hexanes was added. After the addition, the mixture was opened to air and stirred for 5 min, after which TLC analysis showed consumption of 1. The solution was evaporated in vacuo and the residue purified by flash chromatography on SiO₂ (gradient: 95:5 hexanes/EtOAc to 60:40 hexanes/EtOAc) to give 4 mg (33% yield) of 4 as an orange/yellow powder, mp= 210–212° C. R_f = 0.59 (99:1 CH₂Cl₂/MeOH). ¹H NMR (500 MHz, CD₃OD) δ = 7.55 (s, 1H), 7.42 (s, 1H), 7.36 (s, 1H), 7.29 (s, 1H), 6.56 (s, 1H), 6.38 (s, 1H), 4.55

(m, 1H), 3.86 (q, 7.5 Hz, 2H), 2.03 (d, $J = 12.5$ Hz, 2H), 1.89 (t, $J = 12.5$ Hz, 2H), 1.33 (s, 6H), 1.28 (s, 6H) 1.15 (t, $J = 7.5$ Hz, 3H). ^{13}C NMR, HSQC (125 MHz, CD_3OD) $\delta = 149.8$ (4°), 134.9 (CH), 132.6 (CH), 126.8 (4°), 123.2 (CH), 123.1 (4°), 117.8 (CH), 115.1 (CH), 114.2 (CH), 73.7 (O- CH_2), 60.9 (4°), 49.9 (CH), 44.9 (CH_2), 33.3 (CH_3), 21.1 (CH_3), 13.8 (CH_3). IR (cm^{-1}): 3397 (s), 1733 (br, s), 1574 (s), 1462 (m). HRMS (ESI-Orbitrap) m/z : $[\text{M} + \text{H}]^+$ calcd. for $(\text{C}_{20}\text{H}_{30}\text{BF}_2\text{N}_4\text{O})^+$; 391.2472, found 391.2459.

8-*N*-(1-Ethoxy-2,2,6,6-tetramethyl-4-piperidiny)-4,4-difluoro-3,5-dimethyl-4-bora-3a,4a-diaza-*s*-indacene (diMeBODIPY-amino-TEMPOEt 5): To a dry round-bottomed flask equipped with a stir bar was charged 14 mg (0.036 mmol, 1.0 eq.) of diMeBODIPY-amino-TEMPO 2 dissolved in 2 mL of THF. The mixture was stirred for 10 min before 90 μL (0.090 mmol, 2.5 eq.) of 1 M BEt_3 in THF was added. After the addition, the mixture was opened to air via needle tip and left stirring for 25 h, after which TLC analysis showed consumption of 2. The solution was evaporated in vacuo and the residue purified by flash chromatography on SiO_2 (gradient: 95:5 hexanes/EtOAc to 60:40 hexanes/EtOAc). The product was recrystallized from hexanes to give 8 mg (55% yield) of 5 as orange crystals, mp = 188–191° C. $R_f = 0.64$ (99:1 $\text{CH}_2\text{Cl}_2/\text{MeOH}$). ^1H NMR (500 MHz, CD_3OD) $\delta = 7.21$ (s, 2H) 6.19 (s, 2H), 4.40 (tt, $J = 12.0$ Hz, 4.0 Hz, 1H), 3.84 (q, $J = 7.0$ Hz, 2H), 2.47 (s, 6H), 1.99 (d, $J = 12.0$ Hz, 2H), 1.81 (t, 2H, $J = 12$ Hz), 1.30 (s, 6H), 1.26 (s, 6H), 1.14 (t, $J = 7.0$ Hz, 3H). ^{13}C NMR (125 MHz, CD_3OD + a minimal amount of DMSO d_6 was added to increase solubility) $\delta = 47.4$, 123.4 (broad), 118.0 (broad), 116.2 (broad), 115.0 (broad), 73.6, 60.9, 45.1, 33.4, 21.2, 14.6, 14.4, 13.9. IR (cm^{-1}): 3405 (s), 1720 (br, s), 1578 (s), 1417 (s). HRMS (ESI-Orbitrap) m/z : $[\text{M} + \text{H}]^+$ calcd. for $(\text{C}_{22}\text{H}_{34}\text{BF}_2\text{N}_4\text{O})^+$; 419.2785, found 419.2772.

8-*N*-(1-Ethoxy-2,2,6,6-tetramethyl-4-piperidiny)-4,4-difluoro-1,3,5,7-tetramethyl-4-bora-3a,4a-diaza-*s*-indacene (tetMeBODIPY-amino-TEMPOEt 6): To a dry round-bottomed flask equipped with a stir bar was charged 29 mg (0.069 mmol, 1.0 eq.) of tetMeBODIPY-amino-TEMPO 3 dissolved in 20 mL of hexanes and stirred

for 20 minutes before adding 200 μL (0.20 mmol, 2.9 eq.) of 1 M BEt_3 in hexanes. After the addition, the mixture was left stirring for 24 h, then the solution opened to air and a further 200 μL (0.20 mmol, 2.9 eq.) of 1 M BEt_3 in hexanes was added and left stirring for 24 h. Another 400 μL (0.40 mmol, 5.8 eq.) of 1 M BEt_3 in hexanes was added; the solution darkened and TLC analysis showed consumption of **3**. The mixture was evaporated in vacuo and the residue purified by flash chromatography on SiO_2 (isocratic: 9:1 hexanes/EtOAc) to give 17 mg (55% yield) of **6** as an orange powder, mp = 159–160° C. R_f = 0.20 (1:1 CH_2Cl_2 /hexanes). ^1H NMR (500 MHz, CD_3OD) δ = 6.08 (s, 2H), 3.92 (tt, J = 12.0 Hz, 4.0 Hz, 1H) 3.80 (q, 2H, J = 7.0 Hz), 1.93 (d, J = 12.0 Hz, 2H), 1.60 (t, J = 12.0 Hz, 2H), 1.20 (s, 6H), 1.12 (s, 6H), 1.10 (t, 3H, J = 7.0 Hz). ^{13}C NMR, HSQC (125 MHz, CD_3OD) δ = 153.0 (4°), 142.9 (4°), 134.9 (4°), 125.8 (4°), 119.6 (CH), 73.6 (O- CH_2), 61.2 (4°), 55.7 (CH), 47.6 (CH_2), 33.2 (CH_3), 21.2 (CH_3), 15.6 (CH_3), 14.2 (CH_3), 13.7 (CH_3). IR (cm^{-1}): 3414 (s), 1723 (br, s), 1576 (s), 1454 (m). HRMS (ESI-Orbitrap) m/z : $[\text{M} + \text{H}]^+$ calcd. for ($\text{C}_{24}\text{H}_{38}\text{BF}_2\text{N}_4\text{O}$) $^+$; 447.3098, found 447.3080.

Single crystals of **1**, **2**, and **3** were obtained by slow evaporation from CH_2Cl_2 /hexanes. Data were collected on a Bruker APEX II single-crystal X-ray diffractometer. Structures deposited into the Cambridge Structural Database (CCDC 1863622–1863624). UV-Vis measurements were taken in HPLC grade methanol and spectroscopic grade cyclohexane/dichloromethane (7:3 v/v ratio, to prevent precipitation of the marginally soluble nitroxides) on a Shimadzu UV-2700 UV-Vis Spectrofluorometer. Photoluminescence spectra were obtained on a Horiba FluoroMax-4 Spectrofluorometer, with an excitation and emission slit width of 2.5 nm. UV-Vis and fluorescence emission spectra were taken at room temperature. Extinction coefficients were estimated from an average of no less than three separately weighed stock solutions at 100 μM . Relative fluorescence quantum yields were measured using Coumarin 153 as a standard (0.53 in EtOH).¹⁸ Error in relative quantum yields were calculated by propagation of uncertainty in linear regressions of absorption vs. integrated total fluorescence. Nuclear Magnetic

Resonance (NMR) spectra were recorded on a Bruker Avance III HD 4 channel 500 MHz Oxford Magnet NMR spectrometer with Automation or a Bruker Avance III HD 800 MHz NMR Spectrometer. FTIR spectra taken in CHCl_3 and recorded with a Perkin Elmer Spectrum One spectrometer in NaCl microsolution cells. HRMS was recorded with a Thermo Scientific LTQ-Orbitrap Velos Pro MS.

Crystallographic details for **1-3**, additional UV-Vis and Fluorescence spectra, ^1H and ^{13}C NMR spectra for **1-6**

TABLES AND FIGURES

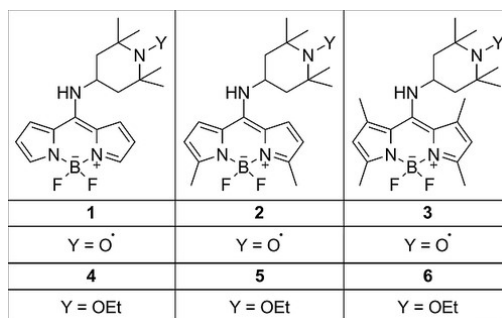


Figure 1. Structure of BODIPY nitroxides **1**, **2**, and **3**, and BODIPY *N*-ethoxyamines **4**, **5**, and **6**

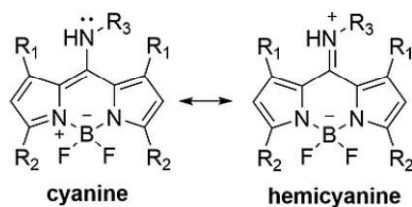
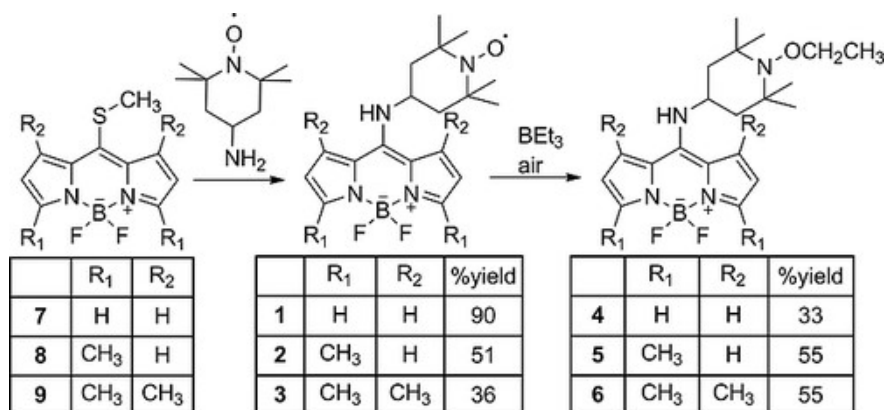


Figure 2. “Hemicyanine” and “cyanine” resonance structures in 8-amino BODIPY dyes.



Scheme 1. Synthesis of profluorescent BODIPY nitroxides **1**, **2**, **3**, and *N*-ethoxyamine derivatives **4**, **5**, and **6**.

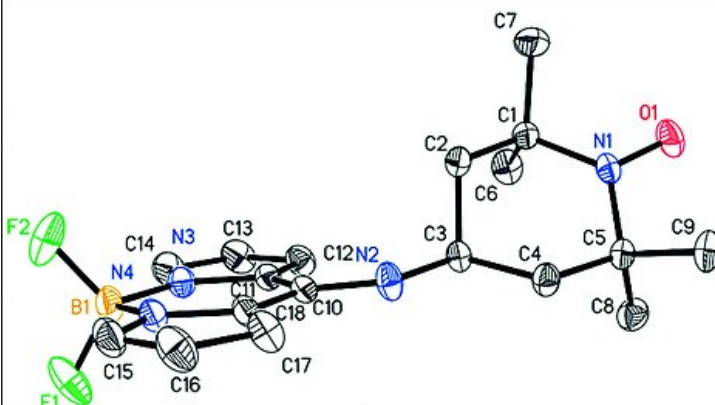
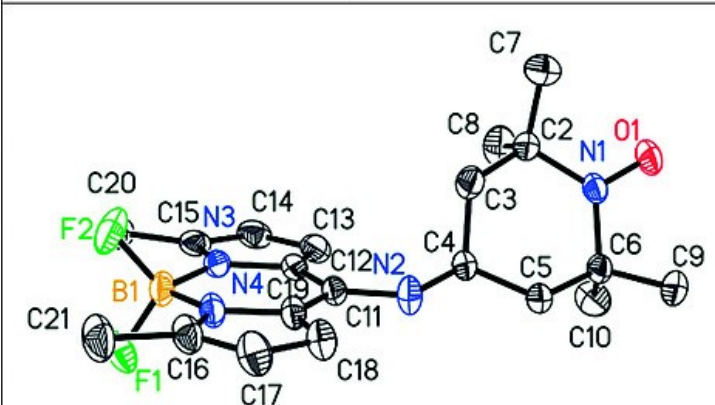
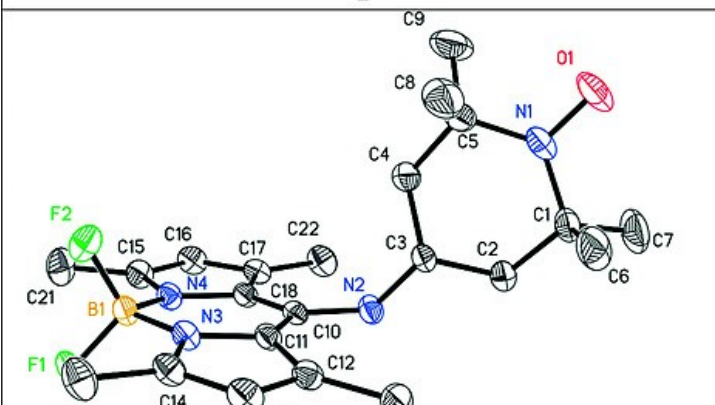
	A dihedral angles	B distances
 <p>ORTEP structure of nitroxide 1, viewed along the BODIPY ring axis. The structure shows a BODIPY core with a nitroxide group (N1-O1) and a fluorophore (B1-F1, F2). Atoms are labeled C1-C18, N1-N4, O1, and B1. Thermal ellipsoids are shown at 50% probability.</p>	$C_3-N_2-C_{10}-C_{11}=3.1^\circ$	$C_{10}-N_2=1.33 \text{ \AA}$ $C_{10}-N_1=5.36 \text{ \AA}$ $B_1-N_1=8.20 \text{ \AA}$
 <p>ORTEP structure of nitroxide 2, viewed along the BODIPY ring axis. The structure shows a BODIPY core with a nitroxide group (N1-O1) and a fluorophore (B1-F1, F2). Atoms are labeled C1-C21, N1-N4, O1, and B1. Thermal ellipsoids are shown at 50% probability.</p>	$C_4-N_2-C_{11}-C_{12}=13.4^\circ$	$C_{11}-N_2=1.34 \text{ \AA}$ $C_{11}-N_1=5.32 \text{ \AA}$ $B_1-N_1=8.15 \text{ \AA}$
 <p>ORTEP structure of nitroxide 3, viewed along the BODIPY ring axis. The structure shows a BODIPY core with a nitroxide group (N1-O1) and a fluorophore (B1-F1, F2). Atoms are labeled C1-C22, N1-N4, O1, and B1. Thermal ellipsoids are shown at 50% probability.</p>	$C_3-N_2-C_{10}-C_{11}=61.1^\circ$	$C_{10}-N_2=1.37 \text{ \AA}$ $C_{10}-N_1=5.25 \text{ \AA}$ $B_1-N_1=7.77 \text{ \AA}$

Figure 3. ORTEP structures and selected parameters of nitroxides **1**, **2**, and **3** from single crystal diffraction data with thermal ellipsoids at 50% probability, viewed along the BODIPY ring axis. **A:** Acute dihedral angles (degrees) between TEMPO methine carbon atom C^3/C^4-N^2 and carbons in BODIPY ring **B:** Bond lengths from *meso* carbon of BODIPY $C^{10}/C^{11}-N^2$, and interatomic distances between nitroxide center N_1 and BODIPY fluorophore atoms C^{10}/C^{11} and B^1 .

compound	λ_{ex} (nm) ϵ (L mol ⁻¹ cm ⁻¹)	λ_{em} (nm)	ϕ_{rel} ^a	$\phi_{\text{NOEt}}/\phi_{\text{NO}^\cdot}$	$\phi_{\text{NOEt}}/\phi_{\text{NO}^\cdot}(0.1\text{mM})$ ^b
1 (MeOH)	405 (20,000)	469	0.090±0.005	-	-
1 (CyH/CH ₂ Cl ₂)	419 (20,000)	469	0.10±0.01	-	-
2 (MeOH)	426 (30,000)	485	0.097±0.006	-	-
2 (CyH/CH ₂ Cl ₂)	439 (30,000)	488	0.047±0.004	-	-
3 (MeOH)	458 (40,000)	492	0.020±0.001	-	-
3 (CyH/CH ₂ Cl ₂)	464 (40,000)	497	0.025±0.002	-	-
4 (MeOH)	402 (20,000)	465	0.031±0.001	0.34	10
4 (CyH/CH ₂ Cl ₂)	415 (20,000)	468	0.69±0.04	6.9	17
5 (MeOH)	424 (30,000)	483	0.58±0.04	6.0	9.9
5 (CyH/CH ₂ Cl ₂)	434 (30,000)	488	0.80±0.07	17	0.97
6 (MeOH)	456 (40,000)	490	0.24±0.01	12	14
6 (CyH/CH ₂ Cl ₂)	459 (40,000)	492	0.21±0.01	8.4	130

Table 1. Summary of spectroscopic properties of BODIPY dyes **1**, **2**, **3**, **4**, **5**, and **6** in MeOH and CyH/CH₂Cl₂ solvents.

^[a] Determined relative to Coumarin 153, $\phi = 0.53$ in EtOH.¹⁸

^[b] Value is not a true quantum yield as absorption/emission behavior is nonlinear at this concentration.

REFERENCES

1. J. P. Blinco, K. E. Fairfull-Smith, B. J. Morrow, S. E. Bottle, *Aust. J. Chem.* **2011**, *64*, 373–389.
2. G. I. Likhtenstein, K. Ishii, S. I. Nakatsuji, *Photochem. Photobiol.* **2007**, *83*, 871-881.
3. J. Matko, K. Ohki, M. Edidin, *Biochemistry* **1992**, *31*, 703.
4. A. G. Coman, C. P. Codruta, A. Paun, A. Diac, N. D. Hadăde, L. Jouffret, A. Gautier, M. Matache, P. Ionita, *New J. Chem.* **2017**, *41*, 7472–7480.
5. J. P. Allen, M. C. Pfrunder, J. C. McMurtrie, S. E. Bottle, J. P. Blinco, K. E. Fairfull-Smith, *Eur. J. Org. Chem.* **2017**, 476–483.
6. A. Loudet, K. Burgess, *Chem. Rev.* **2007**, *107*, 4891–4932.
7. J. Bañuelos, V. Martín, C. F. Azael Gomez-Duran, I. J. A. Córdoba, E. Peña-Cabrera, I. García-Moreno, M. E. Pérez-Ojeda, A. Costela, I. L. Arbeloa, T. Arbeloa, *Chem. Eur. J.* **2011**, *17*, 7261–7270.
8. N. Boens, V. Leen, W. Dehaen, *Chem. Soc. Rev.* **2012**, *41*, 1130–1172; A. C. Benniston, G. Copley, *Phys. Chem. Chem. Phys.* **2009**, *11*, 4124–4131.
9. R. Braslau, F. Rivera, E. Lilie, M. Cottman, *J. Org. Chem.* **2013**, *78*, 238–245.
10. A. Ricci, J. Marinello, M. Bortolus, A. Sánchez, A. Grandas, E. Pedroso, Y. Pommier, G. Capranico, A. L. Maniero, G. Zagotto, *J. Med. Chem.* **2011**, *54*, 1003–1009.
11. T. V. Goud, A. Tutar, J. F. Biellmann, *Tetrahedron* **2006**, *62*, 5084–5091.
12. C. A. Osorio-Martínez, A. Urias-Benavídes, C. F. Azael Gomez-Duran, J. Bañuelos, I. Esnal, I. L. Arbeloa, E. Peña-Cabrera, *J. Org. Chem.* **2012**, *77*, 5434–5438.

13. a. T. Kálai, E. Hideg, J. Jekö, K. Hideg, *Tetrahedron Lett.* **2003**, *44*, 8497–8499;
T. Kálai, . b. K. Hideg, *Tetrahedron* **2006**, *62*, 10352–10360.
14. Z. Wang, J. Zhao, A. Barbon, A. Toffoletti, Y. Liu, Y. An, L. Xu, A. Karata, H. G. Yaglioglu, E. A. Yildiz, M. Havalı, *J. Am. Chem. Soc.* **2017**, *139*, 7831–7842.
15. Y. Liu, S. Liu, Y. Wang, *Chem. Lett.* **2009**, *38*, 588–589.
16. M. Liras, S. Simoncelli, A. Rivas-Aravena, O. Garcia, J. C. Scaiano, E. I. Alarcon, A. Aspeé, *Org. Biomol. Chem.* **2016**, *14*, 4023–4026.
17. K. Xu, A. A. Sukhanov, Y. Zhao, J. Zhao, W. Ji, X. Peng, D. Escudero, D. Jacquemin, V. K. Voronkova, *Eur. J. Org. Chem.* **2018**, 885–895.
18. U. Resch-Genger, M. Spieles, J. Pauli, M. Grabolle, C. Wurth, *Nat. Protocols* **2013**, *8*, 1535–1550.

I

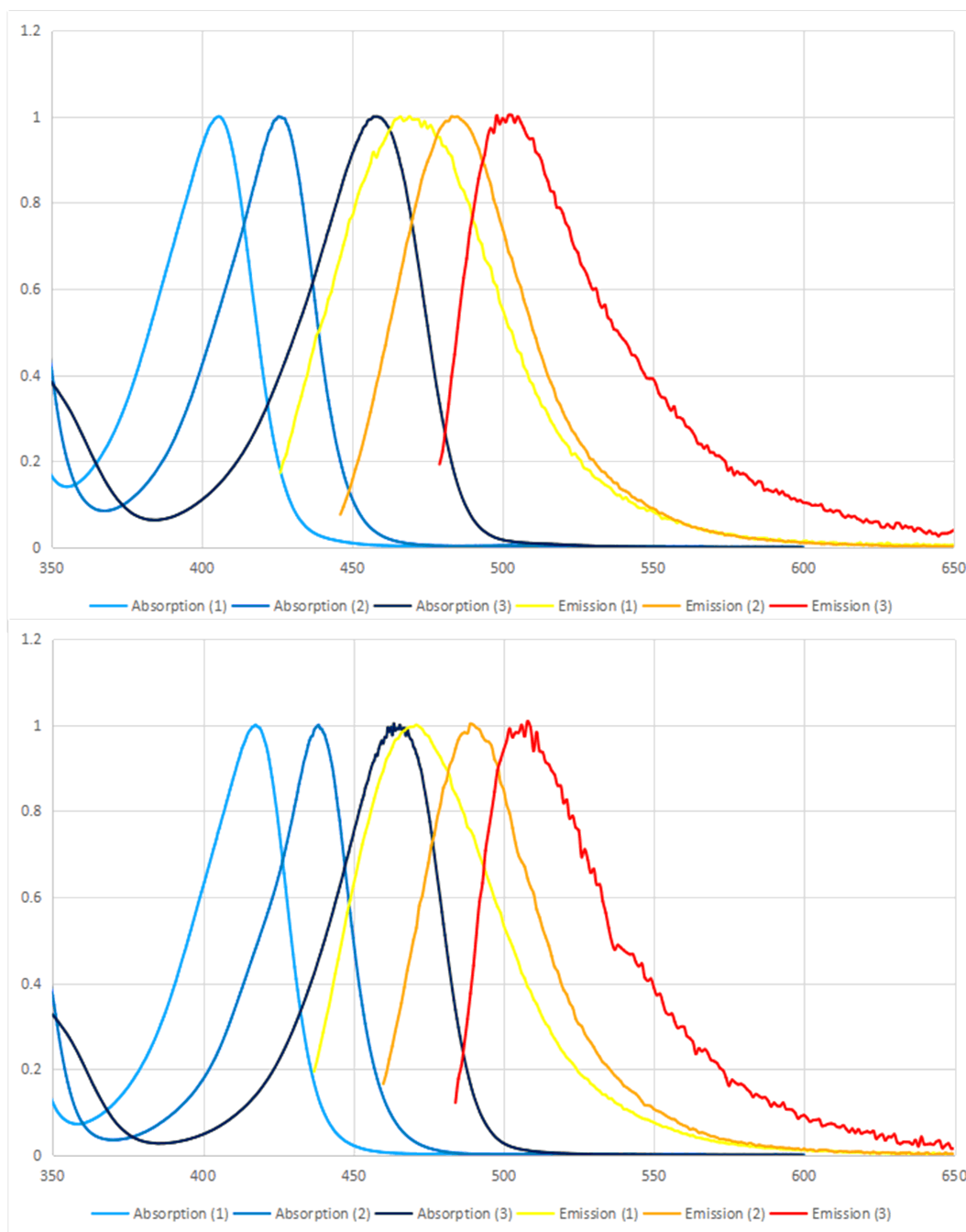


Figure 1. Normalized UV-Vis and fluorescence spectra for nitroxides **1**, **2**, and **3** in MeOH (top) and CyH/CH₂Cl₂ (bottom)

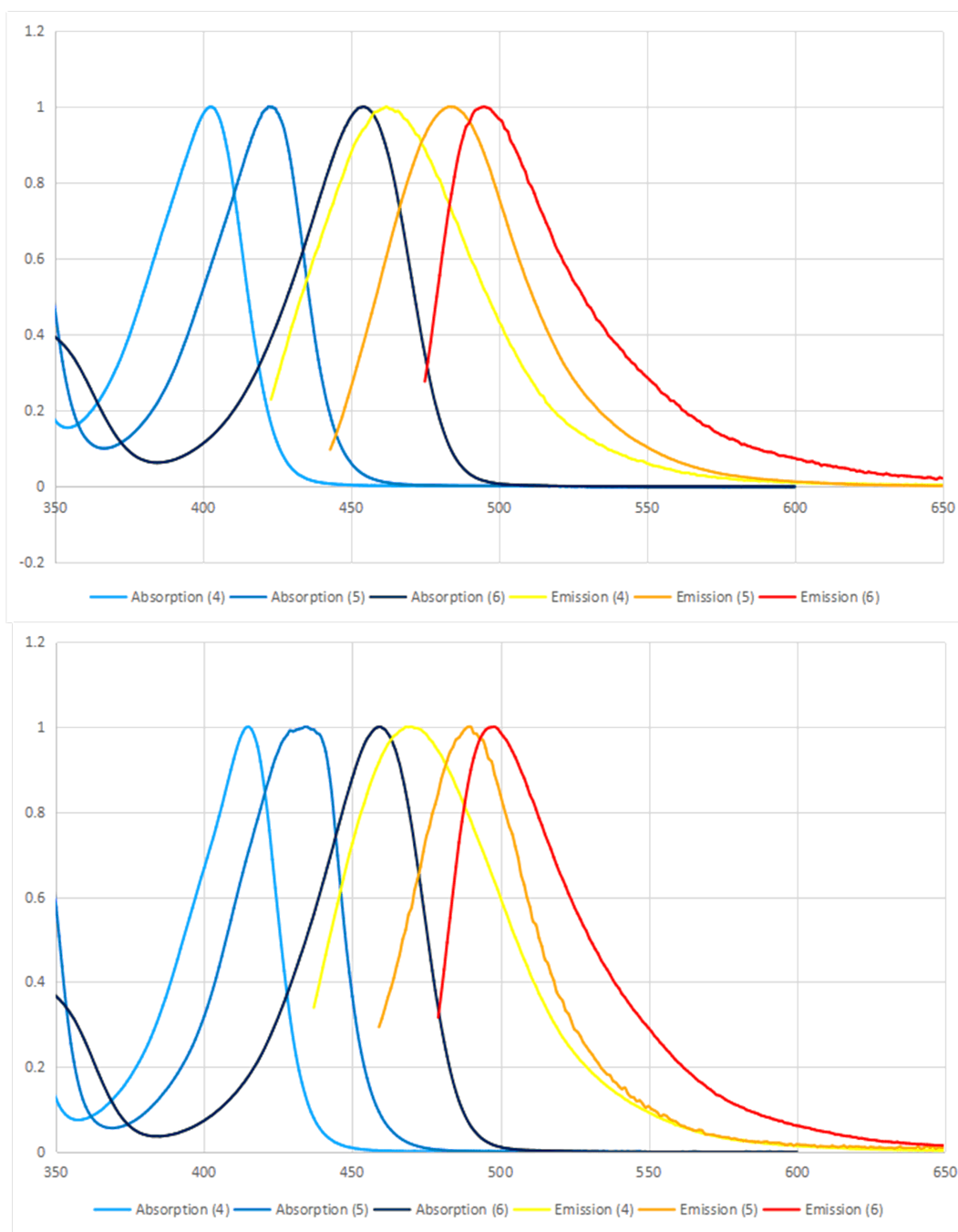


Figure 2. Normalized UV-Vis and fluorescence spectra for *N*-ethoxyamines **4**, **5**, and **6** in MeOH (top) and CyH/CH₂Cl₂ (bottom)

II

General Methods:

Single crystals of **1**, **2**, and **3** were obtained by slow evaporation from CH₂Cl₂/hexanes. Data were collected on a Bruker APEX II single-crystal X-ray diffractometer with graphite-monochromated MoK α radiation ($\lambda = 0.71073 \text{ \AA}$) by a ω -scan technique in the range of $3 \leq 2\theta \leq 50$. Multiscan absorption correction¹ were applied to all of the data sets using SADABS. The structures were generated by direct methods using SHELXT (intrinsic phasing)² and subsequently refined by a full-matrix least-squares procedure on F^2 . In all structures, the H atoms were included in calculated positions on the C atoms to which they are bonded, with C–H = 0.93 \AA and $U_{\text{iso}}(\text{H}) = 1.2U_{\text{eq}}(\text{C})$. Calculations were performed using the SHELXTL 2014³ and Olex2⁴ program packages.

III
Compound 1:

Table 1. Crystal data and structure refinement for xsc1794_0m.

Identification code	xsc1794_0m
Empirical formula	C18 H24 B F2 N4 O
Formula weight	361.22
Temperature	293.15 K
Wavelength	0.71073 Å
Crystal system, space group	Monoclinic, P 1 21/c 1
Unit cell dimensions	a = 10.971(8) Å alpha = 90 deg. b = 11.669(8) Å beta = 96.234(9) deg. c = 14.562(10) Å gamma = 90 deg.
Volume	1853(2) Å ³
Z, Calculated density	4, 1.295 Mg/m ³
Absorption coefficient	0.096 mm ⁻¹
F(000)	764
Crystal size	0.20 x 0.18 x 0.15 mm
Theta range for data collection	2.814 to 24.678 deg.
Limiting indices	-12<=h<=12, -11<=k<=13, -15<=l<=17
Reflections collected / unique	8812 / 3114 [R(int) = 0.0193]
Completeness to theta = 24.678	99.0 %
Absorption correction	Semi-empirical from equivalents
Max. and min. transmission	0.7451 and 0.6858
Refinement method	Full-matrix least-squares on F ²
Data / restraints / parameters	3114 / 0 / 239
Goodness-of-fit on F ²	1.041
Final R indices [I>2sigma(I)]	R1 = 0.0377, wR2 = 0.0931
R indices (all data)	R1 = 0.0445, wR2 = 0.0982
Extinction coefficient	n/a
Largest diff. peak and hole	0.166 and -0.181 e.Å ⁻³

Table 2. Atomic coordinates ($\times 10^4$) and equivalent isotropic displacement parameters ($\text{\AA}^2 \times 10^3$) for xsc1794_0m. U(eq) is defined as one third of the trace of the orthogonalized U_{ij} tensor.

	x	y	z	U(eq)
F(1)	10599(1)	7679(1)	6427(1)	83(1)
F(2)	8825(1)	7825(1)	7072(1)	84(1)
O(1)	4682(1)	2542(1)	2156(1)	52(1)
N(2)	7466(1)	6119(1)	3742(1)	40(1)
N(4)	8779(1)	8161(1)	5445(1)	41(1)
N(3)	9092(1)	6215(1)	6079(1)	41(1)
N(1)	5312(1)	3382(1)	2529(1)	35(1)
C(1)	5450(1)	3422(1)	3559(1)	38(1)
C(2)	5942(1)	4602(1)	3878(1)	38(1)
C(3)	7065(1)	4969(1)	3427(1)	33(1)
C(10)	8073(1)	6468(1)	4532(1)	32(1)
C(18)	8235(1)	7687(1)	4630(1)	36(1)
C(15)	8776(2)	9312(1)	5331(1)	52(1)
C(14)	9439(2)	5353(2)	6668(1)	53(1)
C(13)	9134(2)	4307(2)	6268(1)	53(1)
C(12)	8562(1)	4532(1)	5391(1)	43(1)
C(11)	8534(1)	5722(1)	5270(1)	34(1)
C(16)	8249(2)	9598(2)	4464(1)	57(1)
C(17)	7908(2)	8576(1)	4016(1)	48(1)
C(7)	4183(2)	3252(2)	3879(1)	63(1)
C(5)	6186(1)	3933(1)	1941(1)	34(1)
C(9)	5457(2)	4234(2)	1020(1)	48(1)
C(4)	6697(1)	5046(1)	2392(1)	37(1)
C(8)	7201(2)	3078(2)	1785(1)	48(1)
C(6)	6307(2)	2451(1)	3930(1)	51(1)
B(1)	9341(2)	7493(2)	6286(1)	48(1)

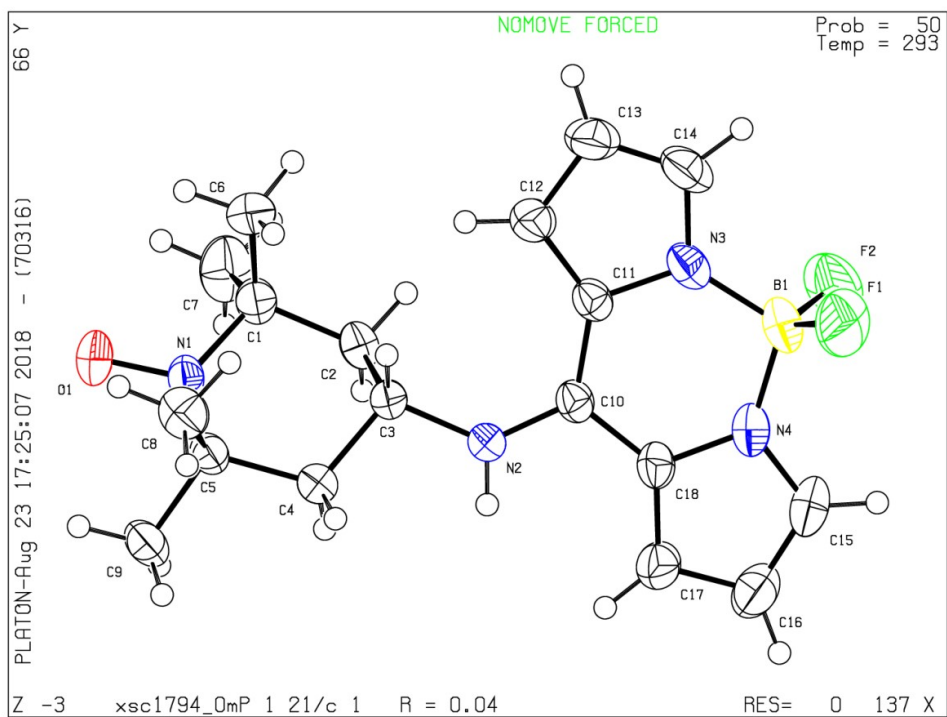


Figure 3. Thermal ellipsoid contour plot for nitroxide **1** (Probability level 50%)

Compound 2:

Table 1. Crystal data and structure refinement for xsc1712_0m.

Identification code	xsc1712_0m
Empirical formula	C40 H56 B2 F4 N8 O2
Formula weight	778.54
Temperature	296.15 K
Wavelength	0.71073 Å
Crystal system, space group	Monoclinic, P 1 21/n 1
Unit cell dimensions	a = 18.5433(17) Å alpha = 90 deg. b = 11.0856(10) Å beta = 109.6900(10) deg. c = 21.364(2) Å gamma = 90 deg.
Volume	4134.8(7) Å ³
Z, Calculated density	4, 1.251 Mg/m ³
Absorption coefficient	0.091 mm ⁻¹
F(000)	1656
Crystal size	0.25 x 0.20 x 0.18 mm
Theta range for data collection	2.522 to 25.061 deg.
Limiting indices	-22<=h<=22, -13<=k<=13, -25<=l<=25
Reflections collected / unique	34787 / 7281 [R(int) = 0.0260]
Completeness to theta = 25.061	99.3 %
Absorption correction	Semi-empirical from equivalents
Max. and min. transmission	0.7452 and 0.6594
Refinement method	Full-matrix least-squares on F ²
Data / restraints / parameters	7281 / 0 / 517
Goodness-of-fit on F ²	1.043
Final R indices [I>2sigma(I)]	R1 = 0.0553, wR2 = 0.1561
R indices (all data)	R1 = 0.0625, wR2 = 0.1621
Extinction coefficient	n/a
Largest diff. peak and hole	0.592 and -0.242 e.Å ⁻³

Table 2. Atomic coordinates ($\times 10^4$) and equivalent isotropic displacement parameters ($\text{\AA}^2 \times 10^3$) for xsc1712_0m. U(eq) is defined as one third of the trace of the orthogonalized Uij tensor.

	x	y	z	U(eq)
F(1)	10718(1)	2213(1)	4671(1)	78(1)
F(3)	1854(1)	6847(2)	2986(1)	82(1)
O(2)	6473(1)	12666(2)	3870(1)	65(1)
F(4)	2574(1)	6620(2)	4068(1)	90(1)
F(2)	10230(1)	2092(2)	3549(1)	90(1)
O(1)	5933(1)	7704(2)	3491(1)	68(1)
N(5)	5987(1)	11811(2)	3679(1)	46(1)
N(8)	3202(1)	6509(2)	3251(1)	48(1)
N(7)	2712(1)	8457(2)	3512(1)	50(1)
N(3)	9895(1)	3814(2)	4083(1)	48(1)
N(6)	4427(1)	8914(2)	3037(1)	49(1)
N(1)	6426(1)	6861(2)	3688(1)	48(1)
N(4)	9372(1)	1783(2)	4165(1)	51(1)
N(2)	8021(1)	4031(2)	4324(1)	57(1)
C(32)	3833(1)	8419(2)	3166(1)	41(1)
C(40)	3297(1)	9081(2)	3375(1)	44(1)
C(25)	4744(1)	10134(2)	3182(1)	41(1)
C(23)	5726(1)	11517(2)	2955(1)	44(1)
C(33)	3754(1)	7143(2)	3080(1)	46(1)
C(12)	9259(1)	4368(2)	4172(1)	44(1)
C(4)	7690(1)	5239(2)	4222(1)	46(1)
C(24)	5328(1)	10294(2)	2830(1)	44(1)
C(5)	7042(1)	5273(2)	4503(1)	48(1)
C(11)	8666(1)	3619(2)	4248(1)	44(1)
C(19)	8742(1)	2347(2)	4248(1)	48(1)
C(26)	5156(1)	10286(2)	3926(1)	46(1)
C(6)	6611(1)	6473(2)	4394(1)	50(1)
C(27)	5542(1)	11508(2)	4126(1)	51(1)
C(2)	6927(1)	6640(2)	3280(1)	51(1)
C(34)	4188(1)	6320(2)	2867(1)	58(1)
C(13)	9378(1)	5610(2)	4187(1)	54(1)
C(39)	3192(1)	10307(2)	3468(1)	55(1)
C(15)	10384(1)	4698(2)	4042(1)	57(1)
C(36)	3298(1)	5315(2)	3151(1)	58(1)
C(18)	8245(1)	1453(2)	4312(1)	59(1)
C(37)	2271(1)	9276(3)	3685(1)	63(1)
C(38)	2557(1)	10421(3)	3658(1)	66(1)
C(16)	9262(1)	575(2)	4170(1)	60(1)
C(14)	10077(1)	5806(2)	4107(1)	62(1)
C(28)	5202(2)	12519(2)	2560(1)	64(1)
C(3)	7343(1)	5446(2)	3474(1)	58(1)
C(35)	3898(1)	5182(2)	2912(1)	65(1)
C(29)	6440(1)	11446(2)	2751(1)	68(1)

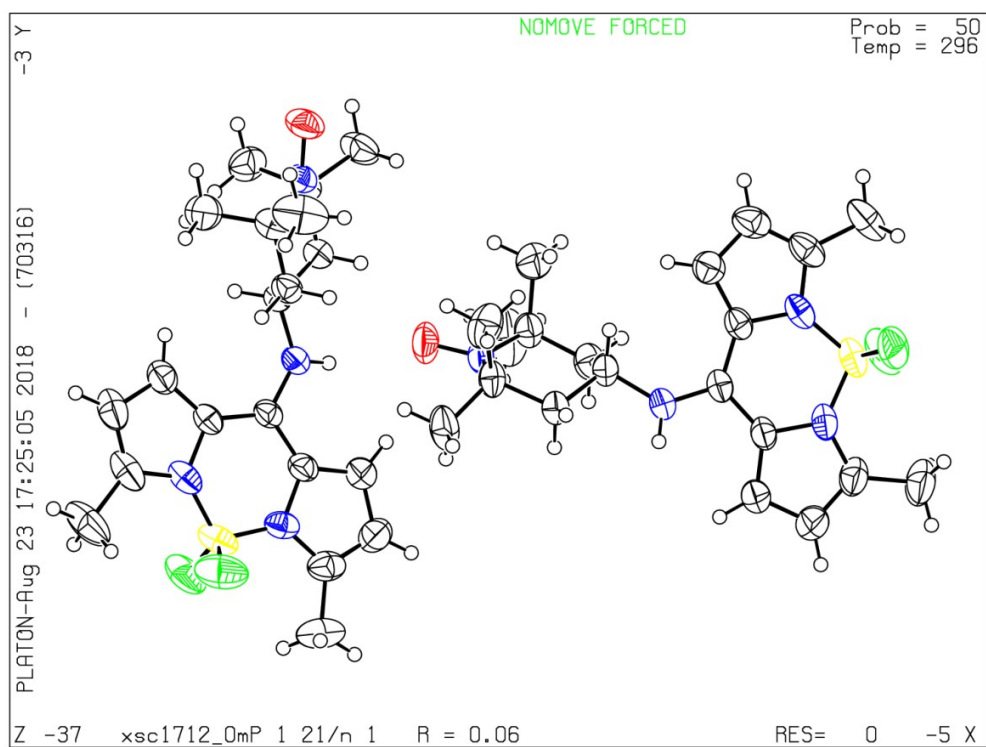


Figure 4. Thermal ellipsoid contour plot for nitroxide **2** (Probability level 50%)

Compound 3:

Table 1. Crystal data and structure refinement for xsc1704_0m.

Identification code	xsc1704_0m
Empirical formula	C ₂₂ H ₃₂ B F ₂ N ₄ O
Formula weight	417.32
Temperature	296.15 K
Wavelength	0.71073 Å
Crystal system, space group	Monoclinic, P 1 2 ₁ /c 1
Unit cell dimensions	a = 12.8258(10) Å alpha = 90 deg. b = 11.0183(8) Å beta = 90.7420(10) deg. c = 16.0536(12) Å gamma = 90 deg.
Volume	2268.5(3) Å ³
Z, Calculated density	4, 1.222 Mg/m ³
Absorption coefficient	0.087 mm ⁻¹
F(000)	892
Crystal size	0.25 x 0.20 x 0.18 mm
Theta range for data collection	2.437 to 24.722 deg.
Limiting indices	-15<=h<=15, -12<=k<=12, -18<=l<=18
Reflections collected / unique	18437 / 3846 [R(int) = 0.0176]
Completeness to theta = 24.722	99.7 %
Absorption correction	Semi-empirical from equivalents
Max. and min. transmission	0.7451 and 0.6822
Refinement method	Full-matrix least-squares on F ²
Data / restraints / parameters	3846 / 0 / 279
Goodness-of-fit on F ²	1.054
Final R indices [I>2sigma(I)]	R1 = 0.0398, wR2 = 0.1050
R indices (all data)	R1 = 0.0457, wR2 = 0.1095
Extinction coefficient	n/a
Largest diff. peak and hole	0.417 and -0.413 e.Å ⁻³

Table 2. Atomic coordinates ($\times 10^4$) and equivalent isotropic displacement parameters ($\text{\AA}^2 \times 10^3$) for xsc1704_0m. U(eq) is defined as one third of the trace of the orthogonalized Uij tensor.

	x	y	z	U(eq)
F(1)	9380(1)	7028(1)	6525(1)	60(1)
F(2)	7815(1)	6242(1)	6881(1)	60(1)
N(3)	8127(1)	6620(1)	5428(1)	38(1)
N(4)	9031(1)	4950(1)	6178(1)	38(1)
N(2)	8295(1)	3928(1)	4071(1)	41(1)
N(1)	5614(1)	2100(1)	3128(1)	52(1)
O(1)	4792(1)	1586(1)	2835(1)	82(1)
C(11)	8065(1)	5889(1)	4716(1)	36(1)
C(10)	8419(1)	4674(1)	4752(1)	35(1)
C(18)	8919(1)	4212(1)	5477(1)	36(1)
C(17)	9315(1)	3046(1)	5686(1)	41(1)
C(3)	7252(1)	3631(1)	3729(1)	38(1)
C(12)	7729(1)	6629(1)	4042(1)	43(1)
C(14)	7822(1)	7755(1)	5214(1)	44(1)
C(13)	7576(1)	7774(2)	4373(1)	50(1)
C(2)	7375(1)	2952(2)	2917(1)	49(1)
C(15)	9468(1)	4283(2)	6797(1)	45(1)
C(16)	9654(1)	3126(2)	6506(1)	48(1)
C(22)	9388(2)	1907(2)	5174(1)	55(1)
C(4)	6650(1)	2840(2)	4324(1)	52(1)
C(1)	6342(1)	2593(2)	2497(1)	52(1)
C(5)	5559(1)	2507(2)	4012(1)	55(1)
C(20)	7639(2)	6342(2)	3132(1)	56(1)
C(19)	7784(2)	8779(2)	5822(1)	60(1)
C(21)	9671(2)	4775(2)	7651(1)	64(1)
B(1)	8582(1)	6234(2)	6278(1)	41(1)
C(6)	5825(2)	3681(2)	2069(1)	80(1)
C(8)	4804(2)	3577(2)	4078(2)	83(1)
C(7)	6552(2)	1589(2)	1863(2)	88(1)
C(9)	5167(2)	1428(3)	4520(2)	95(1)

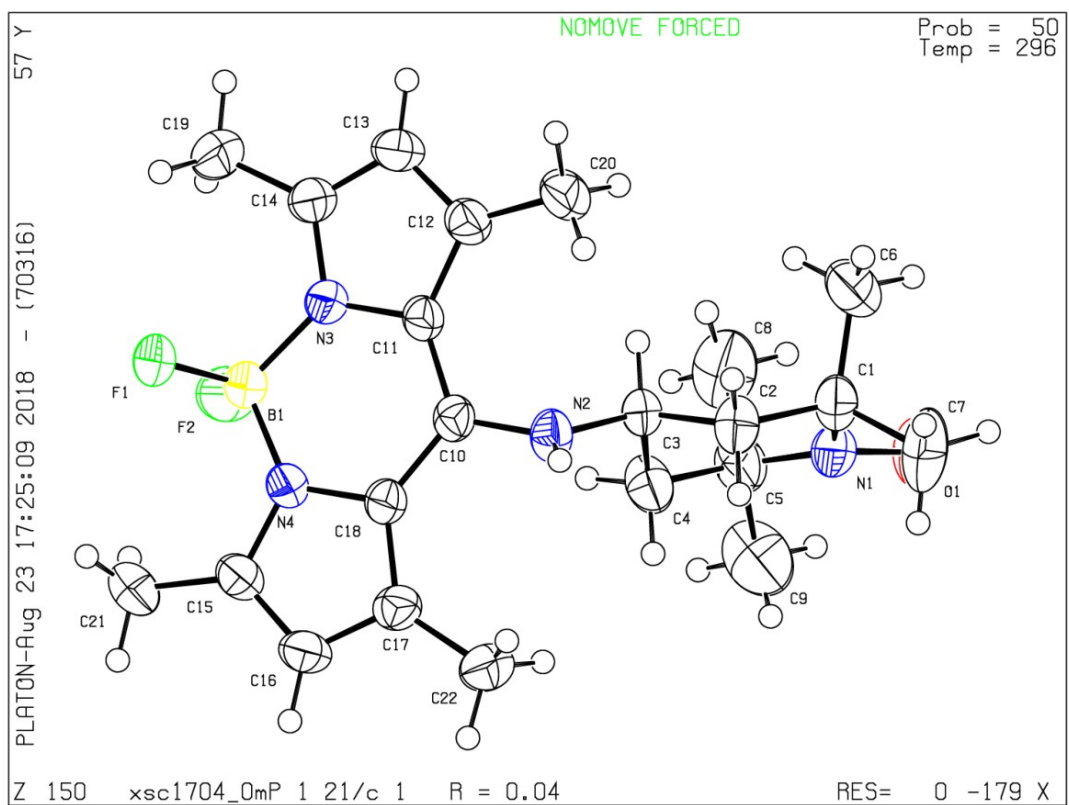


Figure 5. Thermal ellipsoid contour plot for nitroxide **3** (Probability level 50%)

IV

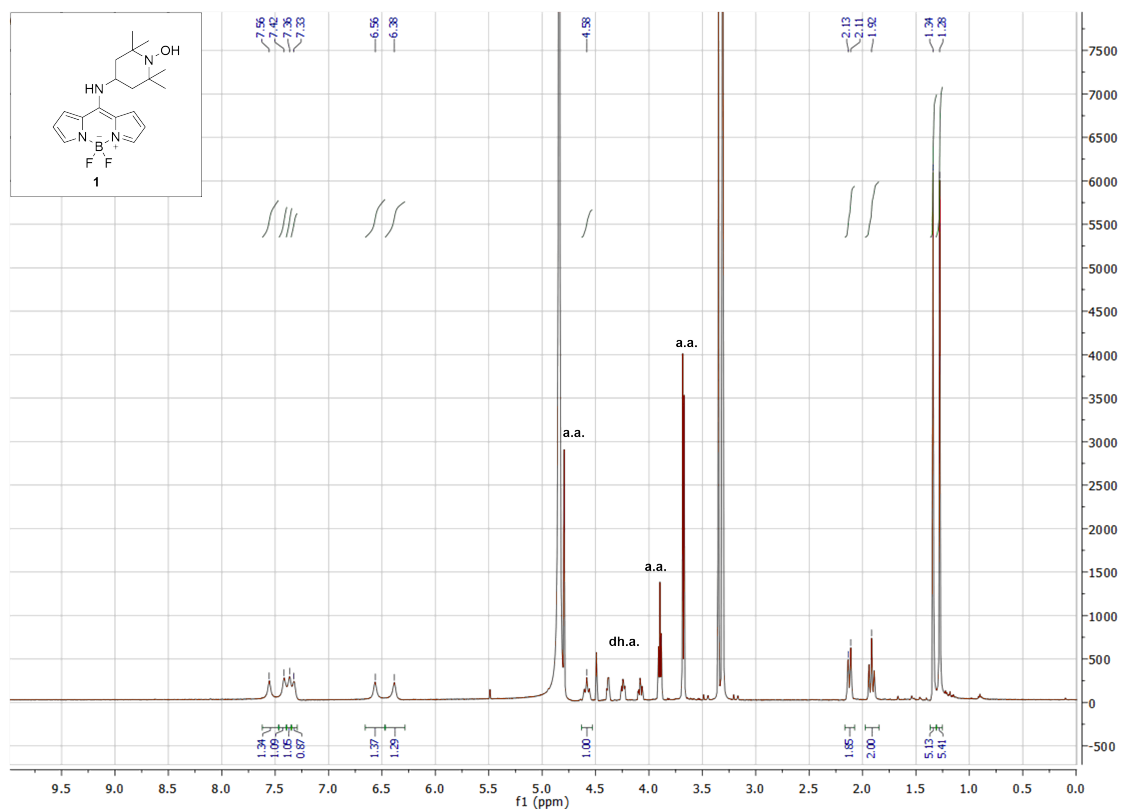


Figure 6: ¹H NMR spectrum of compound **1** in MeOH with ascorbic acid as in situ reductant (a.a.= ascorbic acid, dh.a.= dehydroascorbic acid)

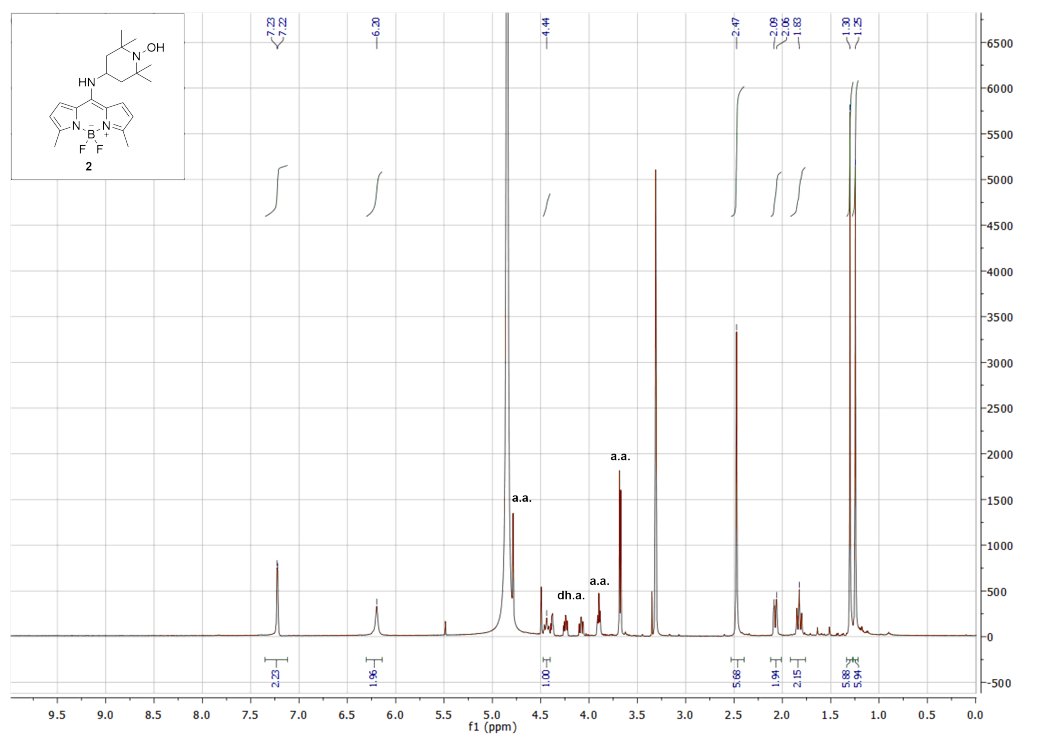


Figure 7: ¹H NMR spectrum of compound 2 in MeOH with ascorbic acid as in situ reductant (a.a.= ascorbic acid, dh.a.= dehydroascorbic acid)

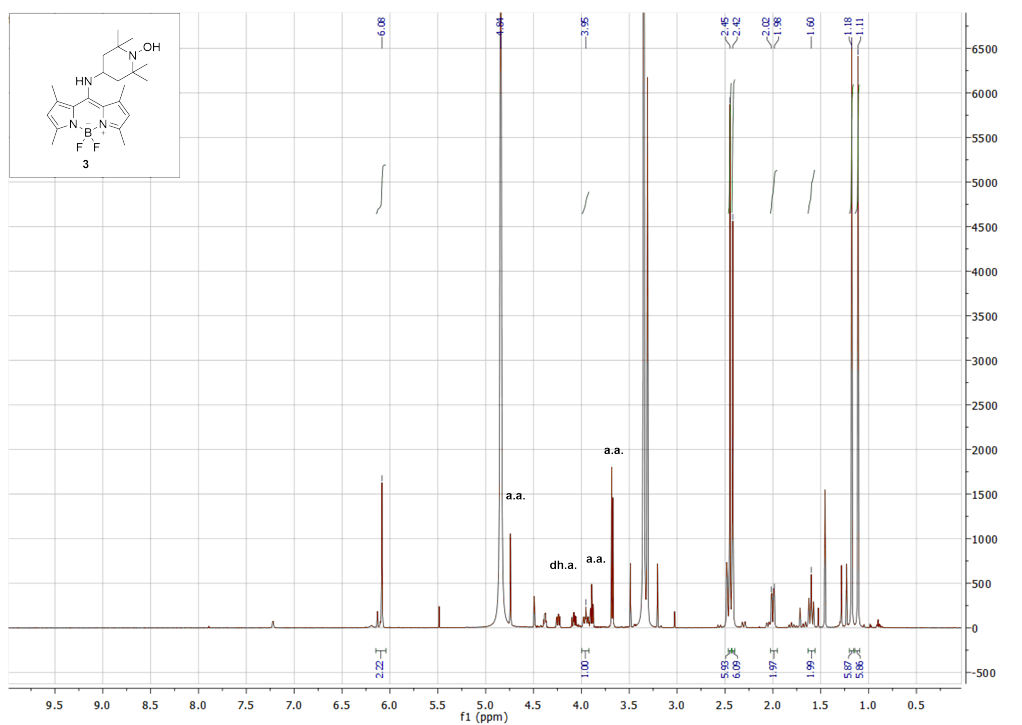


Figure 8: ¹H NMR spectrum of compound **3** in MeOH with ascorbic acid as in situ reductant (a.a.= ascorbic acid, dh.a.= dehydroascorbic acid)

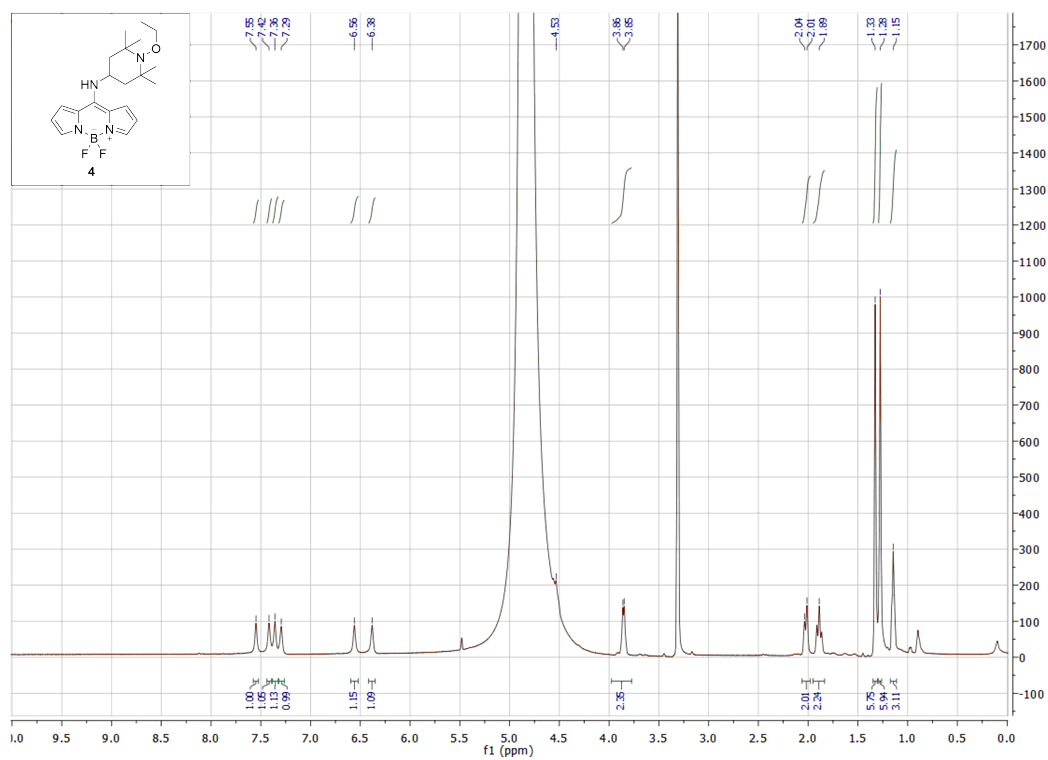


Figure 9: ^1H NMR spectrum of compound **4** in MeOH

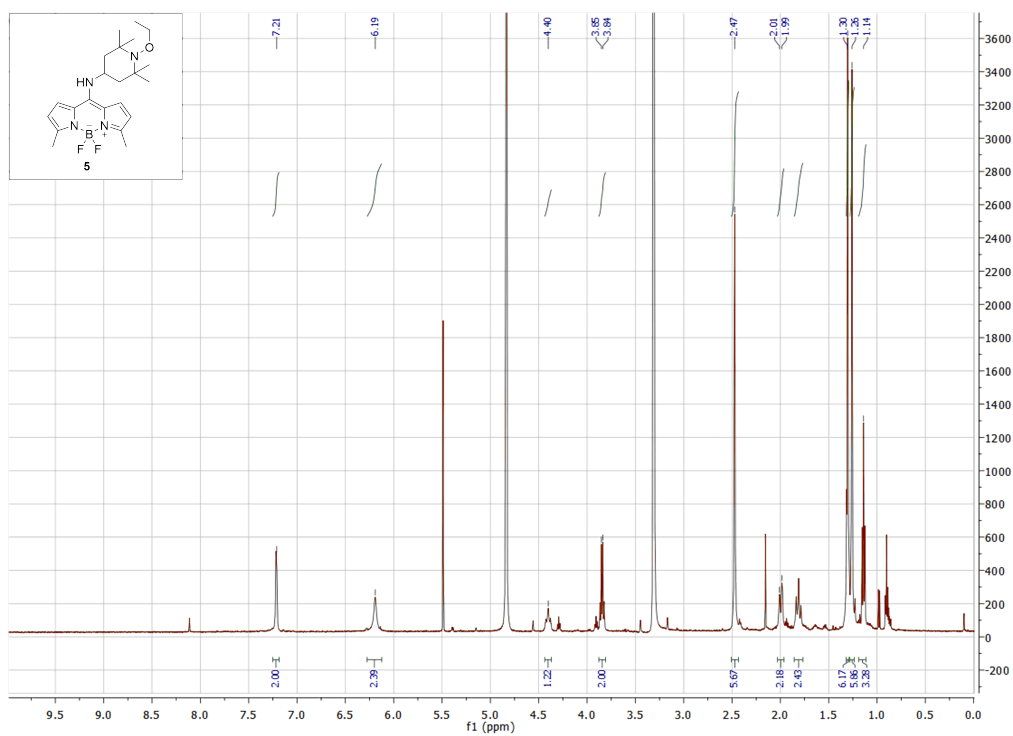


Figure 10: ^1H NMR spectrum of compound 5 in MeOH

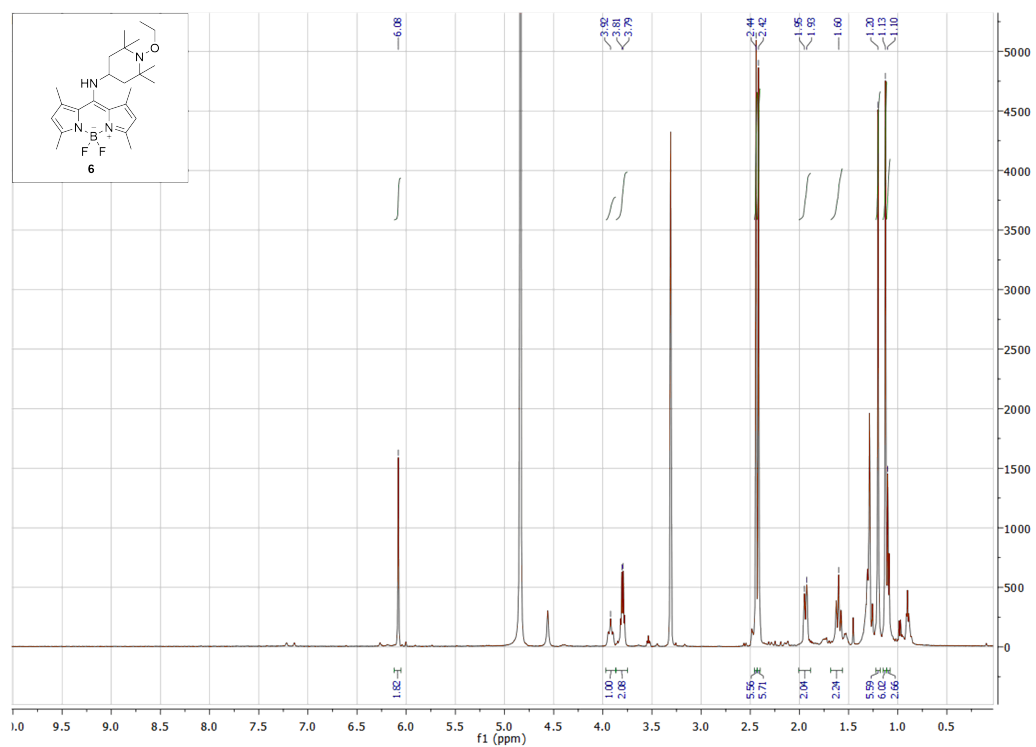


Figure 11: ^1H NMR spectrum of compound **6** in MeOH

V

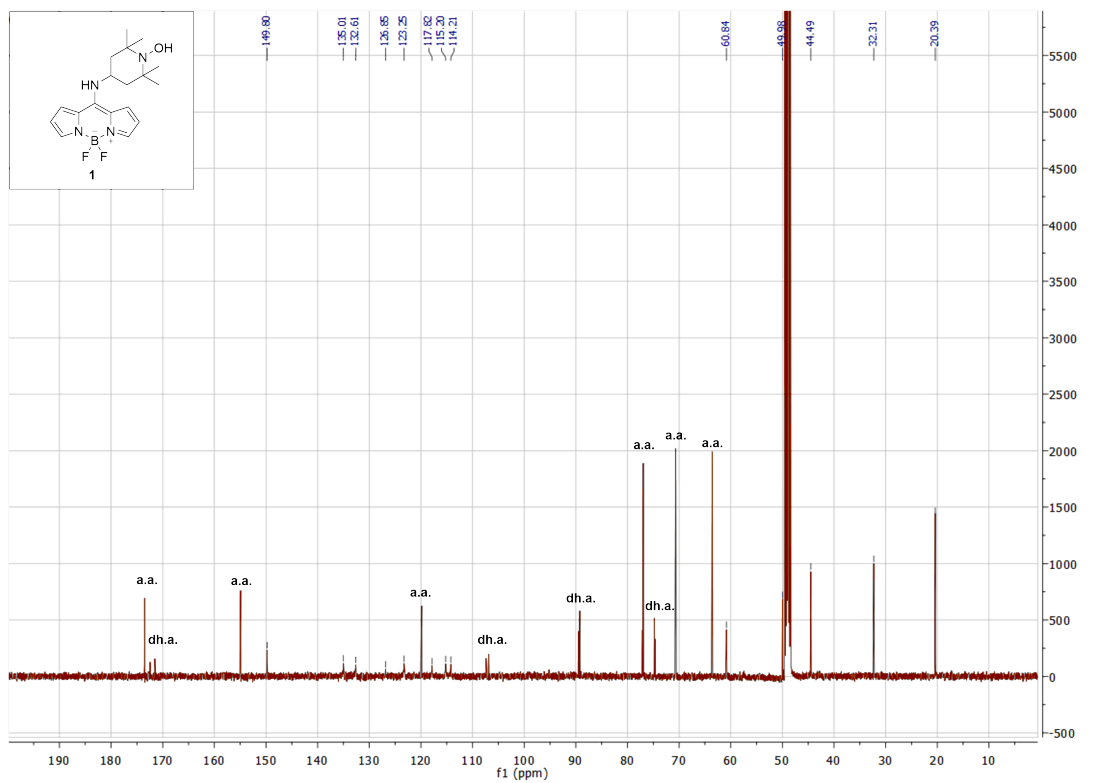


Figure 12: ¹³C NMR spectrum of compound **1** in MeOH with ascorbic acid as in situ reductant (a.a.= ascorbic acid, dh.a.= dehydroascorbic acid)

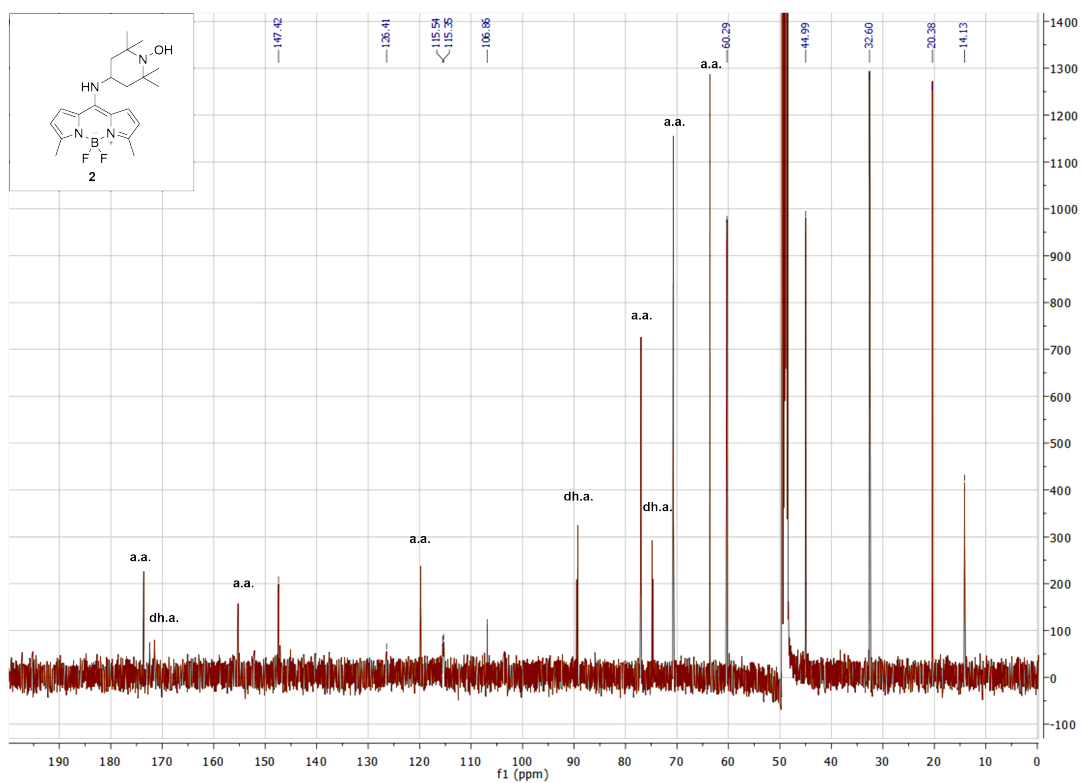


Figure 13: ^{13}C NMR spectrum of compound **2** in MeOH with ascorbic acid as in situ reductant (a.a.= ascorbic acid, dh.a.= dehydroascorbic acid)

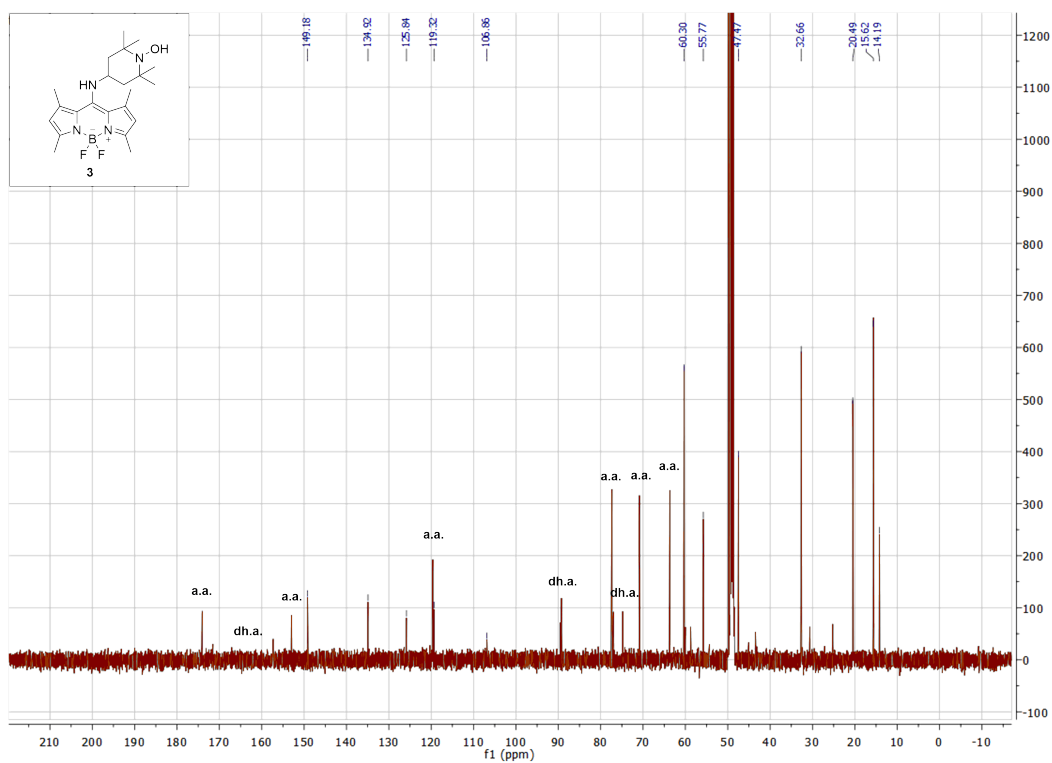
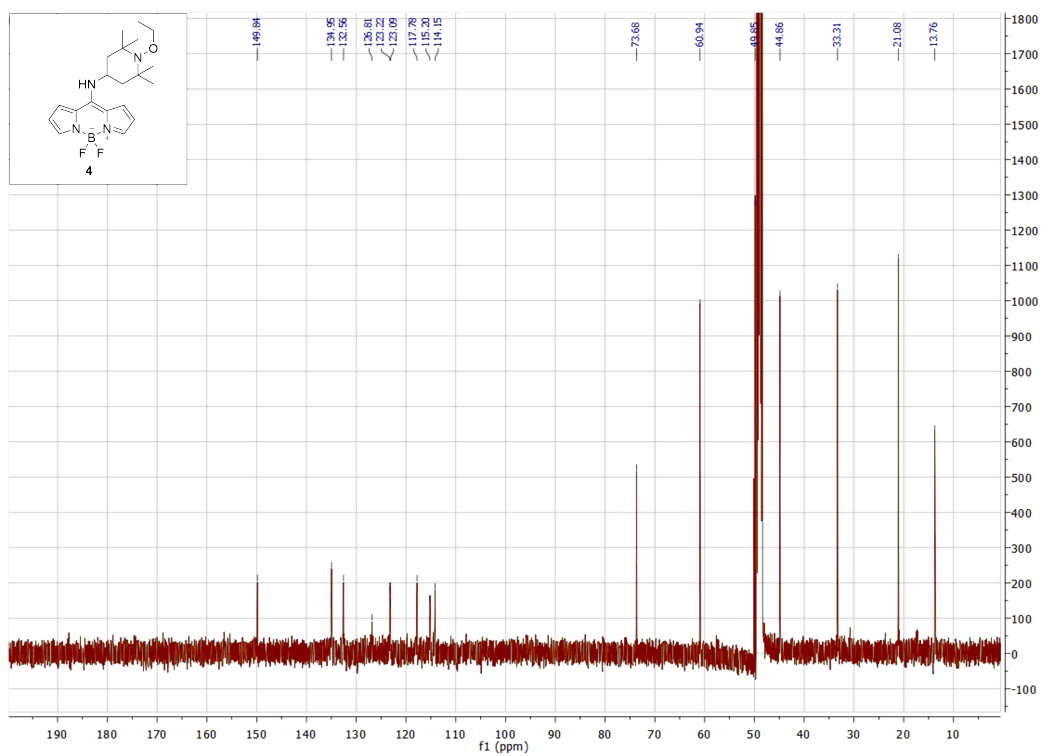
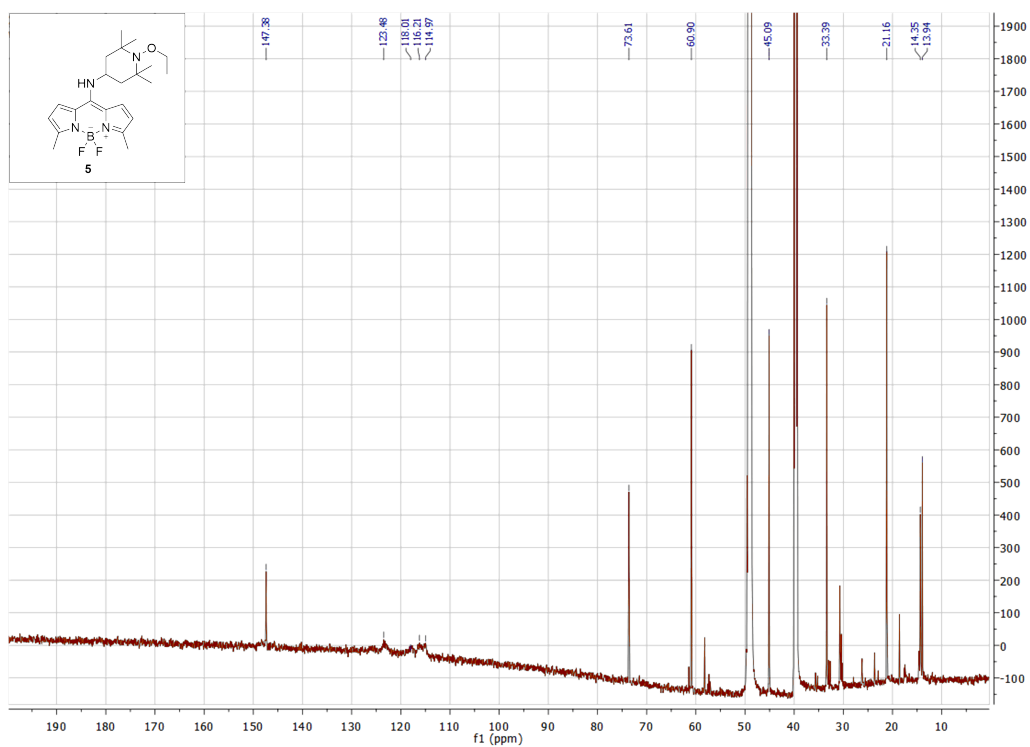


Figure 14: ^{13}C NMR spectrum of compound **3** in MeOH with ascorbic acid as in situ reductant (a.a.= ascorbic acid, dh.a.= dehydroascorbic acid)





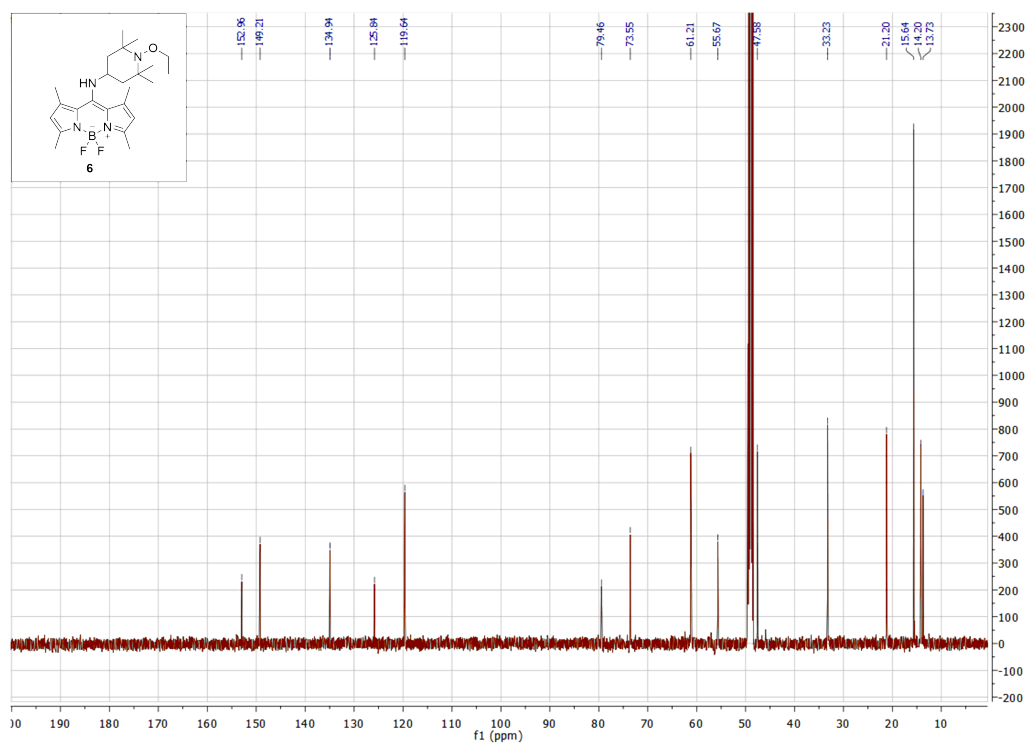


Figure 17: ¹³C NMR spectrum of compound 6 in MeOH

VI
References

1. Blessing, R. H. An empirical correction for absorption anisotropy. *Acta Cryst, Sect. A.* **1995**, *51*, 33–38.
2. Sheldrick, G. M. Crystal structure refinement with SHELXL. *Acta Cryst, Sect. C.* **2015**, *71*, 3-8.
3. Sheldrick, G. M. SHELXT—Integrated space-group and crystal-structure determination. *Acta Cryst, Sect. A.* **2015**, *71*, 3–8.
4. Dolomanov, O. V.; Bourhis, L. J.; Gildea, R. J.; Howard, J. A. K.; Puschmann, H. OLEX2: a complete structure solution, refinement and analysis program. *J. Appl. Cryst.* **2009**, *42*, 339–341.